Polymer Chemistry

Accepted Manuscript

ROYAL SOCIETY OF CHEMISTRY

www.rsc.org/polymers

Journal Name

ARTICLE

Direct synthesis of interface-decorated reactive block copolymer nanoparticles via polymerisation-induced self-assembly

Received 00th January 20xx,
Accepted 00th January 20xx

DOI: 10.1039/x0xx00000x

www.rsc.org/

Yanyan Jiang,[a] Na Xu,[a] Jie Han,[a] Qiuping Yu,[a] Pan Gao,[a] Xinhua Lu[a] and Yuanli Cai[a,*]

Self-assembly of amphiphilic block copolymer in water suffers from the undesired encapsulation of hydrophobic reactive motifs in core-forming block, which deteriorates the performance as aqueous catalysts. This problem can be circumvented by polymerisation-induced self-assembly (PISA). Herein, we report a new strategy for one-pot synthesis of reactive block copolymer nanoparticles whose hydrophobic reactive motifs decorate surrounding core-shell interfaces. We demonstrate fast RAFT aqueous dispersion polymerisation of a commercial available specialty monomer, diacetone acrylamide (DAAM), under visible light irradiation at 25°C. PISA is induced by polymerisation via sequentially dehydration, phase separation and reaction acceleration, and thus complete conversion in 30 min. Replacement of minimal DAAM by NH_3^+-monomer induces slight hydration of the core-forming block, and thus a low polydispersity of resultant statistic-block copolymer. Moreover, simultaneous in situ self-assembly and chain growth favours adjustment of newly-added NH_3^+-units outward to core-shell interfaces while the major DAAM units collapse to hydrophobic PISA-cores. Both lead to timely and selective self-assembly into the new reactive nanoparticles whose NH_3^+-motifs decorate surrounding core-shell interfaces. These nanoparticles well suit fabrication of advanced nanoreactors whose hydrophobic dative metal centres decorate surrounding interfaces via simultaneous imine conversion and Zn(II)-coordination. Such PISA-nanostructures endow hydrophobic metal centres with huge and accessible specific surface area and are stabilized by water-soluble shells. Therefore, this strategy holds fascinating potentials for the fabrication of metalloenzyme-inspired aqueous catalysts.

Introduction

Block copolymer nano-objects have received much attention in recent decades owing to potential applications in drug delivery, cosmetics, catalysis and surface coating.[1-5] However, assembly of amphiphilic block copolymers in water sometimes suffers from undesired encapsulation of hydrophobic reactive motifs in the core-forming block, which deteriorates performance in particular as catalysts.[6-9] Recently, substantial processes have been made by virtue of polymerisation-induced self-assembly (PISA)[3-5] via combination of reversible addition-fragmentation chain transfer (RAFT)[10, 11] with aqueous emulsion/dispersion polymerisation. PISA via aqueous emulsion RAFT, exploited by Hawkett[12, 13] and Charleux,[3, 14, 15] is applicable to hydrophobic monomers.[15-17] In each case, a macromolecular chain transfer agent (macro-CTA) acts as a steric stabilizer, and hydrophobic growing block drives *in situ* self-assembly.

Of most relevance to the present work, PISA by aqueous dispersion RAFT polymerisation was explored in recent years. A pioneering work was reported by Hawker and co-workers.[18] Recently, substantial processes in PISA via aqueous dispersion RAFT have been made by Armes,[19-28] An,[29-31] Sumerlin,[32] and other groups.[5, 33] This approach relies on the use of macro-CTA that is chain-extended by water-soluble monomer into water-insoluble second block, leading to amphiphilic block copolymer that can assemble *in situ* into colloidally stable nano-objects. The convergent growth ensures good colloidal stability due to the steric stabilization of shells, and also is readily amenable to industrial scale-up.[19] Thus, it has quickly become a powerful and versatile technique for the synthesis of nano-objects with well-defined size, morphology and also surface functionality.[5] However, there are rare monomers that meet the criterion of aqueous dispersion RAFT: monomer should be water-soluble while homopolymer must be water-insoluble. The most wide-used monomer is 2-hydroxypropylmethacrylate.[19-28] *N*-Isopropylacrylamide,[18, 32, 34] *N*,*N*-diethylacrylamide,[33] 2-methoxyethyl acrylate,[29, 35] oligo(ethylene glycol)methacrylate[36] are effective to PISA via aqueous dispersion RAFT, typically at 70°C.

Recently, we reported the sequence control over thermo-responsive copolymer based on a ketone-functional monomer, diacetone acrylamide (DAAM).[37] It is a commercially-available specialty monomer that is widely used for the manufacture of various cosmetic products, such as hair conditioners. We have demonstrated that DAAM monomer can be polymerized in a controlled/living manner via RAFT over a wide range of degree of polymerisation (DP=50-1000) in methanol under visible light

[a] The Suzhou Key Laboratory of Macromolecular Design and Precision Synthesis, Department of Polymer Science and Engineering, College of Chemistry, Chemical Engineering and Materials Science, Soochow University, Suzhou 215123, China. E-mail: ylcai@suda.edu.cn; Tel & Fax: +86-512-65884419.

Electronic Supplementary Information (ESI) available: Characterization of PHPMA; photographs of the reaction solutions; light scattering intensity *vs.* concentrations; AEAM homopolymerisation kinetic plots; simultaneous imine conversion/Zn(II)-coordination of AEAM/PDCA compounds. See DOI: 10.1039/x0xx00000x

irradiation at 25°C. Temperature tunable water-solubility was achieved by sequence-controlled copolymerisation with water-soluble *N*,*N*-dimethylacrylamide (DMA). Reorganization can be achieved by post-polymerisation with *O*-benzylhydroxylamine.

We have found that DAAM meets the criterion for aqueous dispersion RAFT because it is water-soluble but homopolymer is water-insoluble even as short as at a DP=50. It prompted us to pursue a PISA via aqueous dispersion RAFT of the monomer. When we almost finished drafting this article, An and co-workers[31] published online a PISA via aqueous dispersion RAFT of the monomer using a $PDMA_{35}$ macro-CTA at 70°C. Uniform nanospheres and vesicles have been achieved. These ketone-containing nanostructures could be functionalized via effective oxime and hydrazone chemistry.

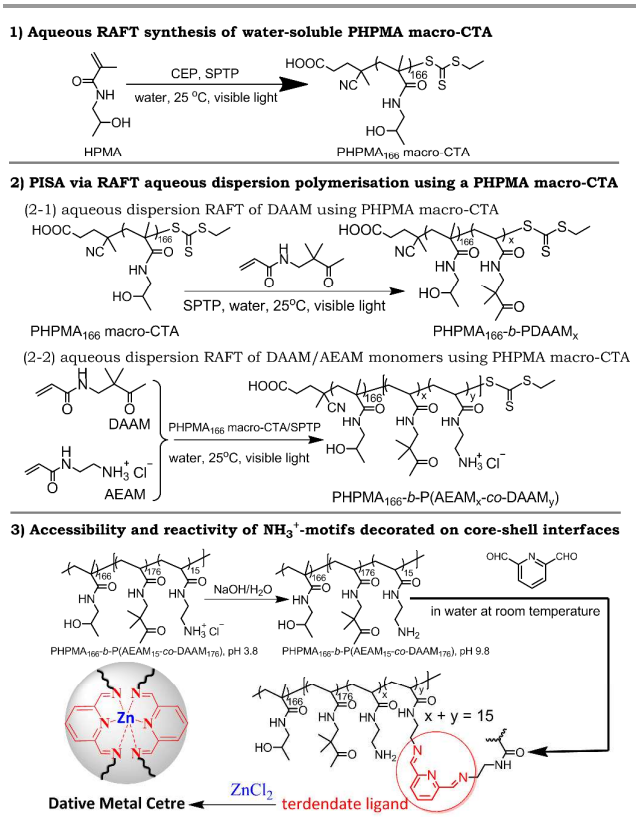

Scheme 1 Schematic illustrations for (**1**) aqueous RAFT synthesis of PHPMA macro-CTA; (**2**) PISA via aqueous dispersion RAFT of DAAM in the absence and presence of minimal AEAM; (**3**) studies on accessibility and reactivity of NH_3^+-motifs in PISA-nanoparticles.

As shown in Scheme 1, this article reports PISA via aqueous dispersion RAFT under visible light irradiation at 25°C. A well-defined poly(2-hydroxypropylmethacrylamide) (PHPMA) was synthesized *via* aqueous RAFT and selected as a macro-CTA. According to McCormick and co-workers,[38] PHPMA is biocompatible and water-soluble. Indeed, a hydration-dependent PISA was observed in aqueous dispersion RAFT of DAAM. Moreover, a new class of reactive nanoparticles was also exploited by the replacement of minimal DAAM by NH_3^+-based *N*-2-aminoethyl acrylamide hydrochloride (AEAM). The reactivity was unveiled by conjugation with pyridine-2,6-dicarboxaldehyde (PDCA) *via* imine bonds to form terdendate ligand motifs, which enables the coordination with ferrous, cobalt, nickel, copper, and zinc ions.[39, 40] Therefore, these PISA-particles are promising as the precursors of metalloenzyme-inspired nanoreactors[6-9] because chemical environment of dative metal centres can be tuned by reaction-induced self-assembly surrounding hydrophobic PISA-cores.[6-8] Zn(II)-coordination was used to illustrate the proof of concept. Polymerisation kinetics, dehydration, phase transition, PISA-structures were studied by ^{1}H NMR, UV-vis spectroscopy, size exclusion chromatography (SEC), dynamic light scattering, atomic force microscopy (AFM) and transmission electron microscopy (TEM). Accessibility of NH_3^+-motifs was probed by ^{1}H NMR and aqueous electrophoresis. Reactivity and reaction-induced reorganization of nanoparticles were also reported.

Experimental Section

Materials

DAAM monomer was donated by Hipro Polymer Materials Co., recrystallized for 2 times from ethyl acetate. 2-Hydroxypropyl methacrylamide (HPMA);[38] *N*-(2-aminoethyl)acrylamide hydrochloride (AEAM);[41] sodium phenyl-2,4,6-trimethylbenzoylphosphinate (SPTP);[42] 4-cyano-4-ethylsulfanylthiocarbonylsulfanyl-pentanoic acid (CEP);[43] these materials were synthesized and purified according to literatures. PDCA was purchased from TCI; $ZnCl_2$ was from Aladdin; deuterium oxide (D_2O, 99.8%D) and methanol-d_4 (99.8%D, 0.03%TMS) were from J&K; deuterchloric acid (DCl, 99.5%D, 20% in D_2O) and sodium deuteroxide (NaOD, 99.5%D, 40% in D_2O) were from Adamas; these agents were used as received. Deionized water (R > 18.2 mΩ/cm) was obtained from an AQUELX 5 Millipore system.

Visible light source

A 400-W mercury lamp was employed for this purpose. JB400 filters were used to filter UV light (λ_{cm} < 400 nm) and decrease intensity to I_{420nm}=0.20 mW/cm^2, which corresponds to ca. 5% of solar irradiation on a typical cloudless day at noon in May in East China. The light intensity was determined using a UV-A radiometer that was equipped with a λ=420 nm detector.

Synthesis of poly(2-hydroxypropyl methacrylamide) macro-CTA

A typical protocol for the synthesis of $PHPMA_{166}$ macro-CTA is as follows: HPMA monomer (8.0 g, 55.9 mmol) and CEP chain transfer agent (58.8 mg, 0.22 mmol) was dissolved in butoxyethanol (2.40 g) in a 50 mL flask. SPTP initiator (17.3 mg, 56 µmol) and water (5.60 g) and was added. The flask was sealed with rubber septa and immersed into water bath at 25°C. The solution was bubbled with argon gas in the dark for 60 min and irradiated with visible light for 80 min. Reaction was quenched by exposure to air. ^{1}H NMR revealed 65% HPMA monomer was polymerized. Reaction solution was precipitated into acetone, washed 3 times in the precipitation solvent, and dried under vacuum at 25°C for 3 days. ^{1}H NMR analysis indicated a DP of 166 for this macro-CTA; DMF SEC analysis indicated the M_n and M_w/M_n values of 40.0 kDa and 1.13, respectively (Electronic Supporting Information, ESI, Fig. S1).

Aqueous dispersion RAFT polymerisation of DAAM monomer

A typical protocol is as follows: DAAM monomer (0.35 g, 2.07 mmol), $PHPMA_{166}$ macro-CTA (0.25 g, 10.3 μmol) and water (3.46 g) was dissolved in a 10-mL flask. SPTP initiator (1.0 wt% in water, 80.3 mg, 2.59 μmol) was added. This flask was sealed and then immersed into a water bath at 25°C. Solution was bubbled with argon gas in the dark for 60 min, and irradiated with visible light. Samples were taken at different time points. The reaction was quenched by exposure to air and addition of hydroquinone inhibitor.

Aqueous dispersion RAFT copolymerisation of DAAM and AEAM

A typical protocol is as follows: $PHPMA_{166}$ (0.28 g, 11.6 μmol), DAAM (0.35 g, 2.07 mmol), AEAM (34.6 mg, 0.23 mmol) and water (3.84 g) was dissolved in a 10 mL flask. SPTP initiator (1.0 wt% in water, 89.2 mg, 2.9 μmol) was added in the flask. This flask was sealed and immersed into water bath at 25°C. The solution was bubbled with argon gas in the dark for 60 min and irradiated with visible light. Samples were taken at different time points. The reaction was quenched by exposure to air and addition of hydroquinone inhibitor.

Simultaneous imine conversion and Zn(II)-coordination of the NH_2-motifs of PISA-micelles: ^{1}H NMR evidence

The reaction solution of PISA-micelles after final conversions at $[AEAM]_0/[DAAM]_0$=20/180 was dialyzed and then lyophilized. ^{1}H NMR in methanol-d_4 indicated pure $PHPMA_{166}$-*b*-P($AEAM_{15}$-*co*-$DAAM_{176}$) (Fig. S8); SEC indicated a polydispersity index (PDI, M_w/M_n) of 1.24. The solids (10.0 mg, [AEAM]=2.7 μmol) were dispersed in D_2O (4.99 g) to a 2.0 mg/mL ($[AEAM]_0$=0.54 mM). The solution was adjusted to pH 3.8 using DCl (1.0 mM in D_2O). Stock solutions of PDCA (2.0 mM) and $ZnCl_2$ (4.0 mM) in D_2O also were prepared. The stock solutions of PISA-micelles (2.0 g, [AEAM]=1.1 μmol), PDCA (0.11 g, 0.22 μmol), $ZnCl_2$ (27.5 mg, 0.11 μmol) and D_2O (1.86 g) were added in a 10-mL vial. The reaction solution was adjusted to pH 9.8 using NaOD (2.0 mM in D_2O). Reaction was probed by ^{1}H NMR after equilibration at 25°C for 2 days.

^{1}H NMR spectroscopy

^{1}H NMR spectra either in methanol-d_4 or in D_2O were acquired on an INOVA 400 MHz NMR instrument, measured at 25°C.

UV-visible spectroscopy

UV-vis spectra were recorded with a Shimadzu UV-3600 UV-vis spectrometer at 25°C.

Size exclusion chromatography (SEC)

Molecular weights (M_n) and polydispersity indices (PDI, M_w/M_n) were determined by a PL-GPC220 integrated system equipped with a refractive index detector and a set of columns (2×PLGel MIXED-B+1×PLGel MIXED-D). The eluent was HPLC-grade DMF that contained 10.0 mM LiBr, which was filtered before use. Near-monodisperse poly(methyl methacrylate) (Agilent, 7.36-2136.0 kDa) were used as standards for the calibration. All the calibration and analysis were carried out at a 1.0 mL/min flow rate and 80°C. To avoid absorption of NH_3^+-motifs onto column materials, samples that contained AEAM units were protected by reaction with methyl acrylate under procedures described by Armes and co-workers.[44, 45]

Aqueous electrophoresis

Zeta potentials (ζ) of PISA-micelles were assessed by aqueous electrophoresis on a Malvern Zetasizer Nano-ZS90 instrument. As-obtained solids of PISA micelles were dispersed in water to 1.0 mg/mL and then adjusted to pH 3.8 using 1.0 mM HCl.

Dynamic light scattering (DLS)

DLS studies were performed on a Brookhaven BI-200SM setup equipped with a 22-mW He-Ne laser (λ=633 nm), a BI-200SM goniometer and a BI-TurboCorr digital correlator. The solution was controlled at 25±0.02°C using BI-TCD controller, measured at a scattering angle of 90°. Otherwise mentioned, the laser intensity was decreased to 50% of the initial. The intensity-averaged hydrodynamic diameters (D_h) and dispersity (μ_2/Γ^2) were assessed by cumulants analysis in CONTIN routine.

Atomic force microscopy (AFM)

AFM was carried out using a Bruker Multimode 8 microscope operated in a peak force quantitative nanomechanical mode using a SCANASYST-AIR probe (spring constants: 0.4 N/m, resonance frequency: 70 kHz, tip radius: 2 nm). Silicon wafer was washed by immersing into the mixture of 98% H_2SO_4 and 35% H_2O_2 (7:3, v/v) for 2 h, and thoroughly rinsed with water. As-cast solution on silicon wafer was lyophilized in a Labconco Freezone2.5L freeze-drier.

Transmission electron microscopy (TEM)

TEM imaging was performed on a Hitachi HT7700 transmission electron microscope at an accelerating voltage of 120 kV. As-cast solution on carbon film-coated copper grid was lyophilized in a Labconco Freezone2.5L freeze-drier.

Results and discussion

Our recent results demonstrated that visible light irradiation could induce ultrafast aqueous RAFT polymerisation at 25°C.[46] This reaction can be commenced and suspended immediately by turning on-off visible light,[47, 48] such that chain length can be finely tuned during the chain extension.[41] In this article, we use this technique to elucidate the PISA via aqueous dispersion RAFT of commercially available specialty monomer DAAM[31, 37] under visible light irradiation at 25°C. To this end, sodium phenyl-2,4,6-trimethylbenzoylphosphinate (SPTP) was selected as photoinitiator, which was synthesized according to a patent procedure.[42] It is a weak acid (pKa=6.50) and has a broad peak of $n\rightarrow\pi^*$ transition at λ_{max}=371 nm.[41] The lithium salt was used as the photoinitiator to prepare cell scaffolds,[49] extracellular mimics[50] and hydrogels.[51] After trying a variety of free radical initiators, SPTP was proven to be the most effective in terms of the initiation and chain propagation in response to visible light irradiation in aqueous solutions at room temperature.[41]

Scheme 1 shows the synthesis of poly(2-hydroxypropylmethacrylamide) (PHPMA) macro-CTA *via* aqueous RAFT under visible light irradiation at 25°C. Degree of polymerisation was targeted at DP_{target}=250, $[HPMA]_0/[CEP]_0$=250, $[CEP]_0/[SPTP]_0$= 4.0. The reaction was quenched after the irradiation for 80 min. ^{1}H NMR indicated 65% conversion. This reaction solution was precipitated into acetone and dried to afford a final DP of 166, judged by ^{1}H NMR (Fig. S1). This macro-CTA have M_n=40 kDa and M_w/M_n=1.13, judged by SEC analysis (Fig. S1). Taking into account DP_{target}=250 and 65% conversion, a high CTA-efficiency of 98% was assessed within the analysis errors. High fidelity of CTA chain-ends was confirmed by below-discussed formation of well-defined block copolymers.

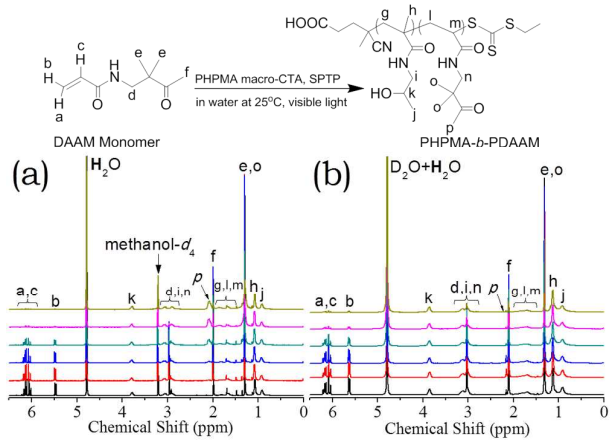

Fig. 1 the evolution of ^{1}H NMR spectrum on aqueous polymerisation at $[DAAM]_0$=0.5 M, $[DAAM]_0/[PHPMA_{166}]_0/[SPTP]_0$=200/1/0.25 under visible light irradiation for 0, 5, 10, 16, 22, 24 min (*from bottom to top*), in which spectra were recorded in methanol-d_4 (**a**) and D_2O (**b**). *Top*: Schematic illustration of the polymerisation.

Polymerisation-induced self-assembly: hydration effect

As shown in Scheme 1, PISA proceeded *via* aqueous RAFT of DAAM at $[DAAM]_0$=0.5 M, and DP_{target}=200 and 100, using a $PHPMA_{166}$ macro-CTA and SPTP initiator in water at pH 3.8 under visible light irradiation at 25°C. As shown in Fig. 1a, the proton signals of DAAM and PHPMA are completely discernible in methanol-d_4. Upon irradiation, the C**H**=C**H**$_2$ signals *a*, *b* and *c* decreased, and the signal *p* (COC**H**$_3$ in DAAM unit) increased. The C**H**=C**H**$_2$ signals virtually disappeared in 24 min, indicating fast polymerisation. The monomer conversions were assessed using the integral signal *k* as a standard according to Eq. 1, in which $I_{b,0}$ and $I_{k,0}$ are the initial integral signals *b* and *k*; $I_{b,t}$ and $I_{k,t}$ are those at different irradiation time points.

$$Conversion = \left(1 - \frac{I_{b,t}}{I_{k,t}} \times \frac{I_{k,0}}{I_{b,0}}\right) \times 100\% \quad (1)$$

Moreover, degree of dehydration of the polymeric DAAM units was determined by ^{1}H NMR in D_2O. As shown in Fig. 1b, the signal *p* is weaker than that in methanol-d_4 (Fig. 1a), which suggest that DAAM units have been dehydrated during the chain extension. Because the signal *p* overlaps with the signal *f*, polymerisation-induced dehydration was determined using the integral signal *n* (CONHC**H**$_2$ in DAAM unit) according to Eq. 2, in which $I_{k,0}$, $I_{(d+i),0}$ are initial integral signals *k*, *d*+*i*; $I_{(d+i+n),t}$, $I_{k,t}$ are those of *d*+*i*+*n*, *k* at different time points; DAAM conversions as determined in methanol-d_4 by Eq. 1 were used herein.

$$Dehydration = \left(1 - \frac{I_{(d+i+n),t} - 2 \times I_{k,t}}{I_{(d+i),0} - 2 \times I_{k,0}} \times \frac{I_{k,0}}{I_{k,t}}\right) \times \frac{1}{conversion} \times 100\% \quad (2)$$

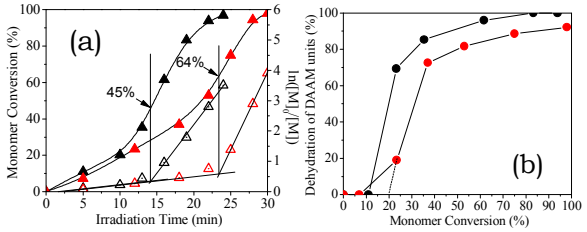

Fig. 2 (**a**) Kinetic plots of RAFT polymerisation in acidic water at a $[DAAM]_0$=0.5 M and $[DAAM]_0/[PHPMA_{166}]_0/[SPTP]_0$=200/1/0.25 (*black*) and 100/1/0.25 (*red*) under visible light irradiation at 25°C; (**b**) dehydration of DAAM units with monomer conversions.

As shown in Fig. 2a, the extremely high conversions (>97%) were achieved upon irradiation within 30 min due to fast and effective polymerisation. Moreover, at a DP_{target}=200, reaction was accelerated after 45% conversions. It is a typical character of PISA, as reported by Armes and co-workers.[19, 27] In contrast, onset of acceleration shifts to 64% conversion at a DP_{target}=100. As shown in Fig. 2b, at DP_{target}=200, their DAAM units started dehydration abruptly at 10% conversion and complete after reaching 80% conversions. At a DP_{target}=100, the dehydration started after 20% conversions. The added DP_{DAAM} are perfectly comparable at these critical conversions in both the reactions. DAAM units completely dehydrated at DP_{target}=200 but slightly hydrated at DP_{target}=100 up to 98% conversions. This indicates that the dehydration depends on PDAAM chain-length.

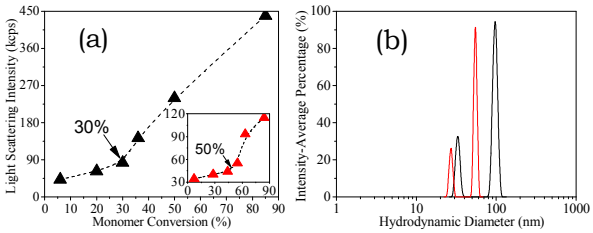

Fig. 3 (**a**) the variation of light scattering intensity upon polymerisation at a DP_{target}=200 (*black*) and 100 (*red*) under the conditions of Fig. 2, where laser was decreased down to 20%; (**b**) the size distribution profiles of PISA-micelles formed at 98% conversions.

PISA-induced phase separation was thus monitored by DLS. As shown in Fig. 3a, at DP_{target}=200, light scattering intensity increased significantly after 30% conversions, which suggests the phase transition from water. This transition is behind as-mentioned start of dehydration but ahead of onset of reaction acceleration. These results indicate that PISA process occurred through sequentially dehydration, phase transition, reaction acceleration. Same sequence was also observed in reaction at DP_{target}=100. Similar observations were reported by the groups of Armes[19, 27] and Zhang[52, 53] in either water, organic solvent or the mixture, which suggest that the residual monomers were

enriched into the hydrophobic PISA-domains, which led to the reaction acceleration.

Reaction solution at DP_{target}=200 changed from transparent to bluish and finally to milky at the extremely high conversions, while reaction at DP_{target}=100 to 98% conversions just led to a bluish transparent solution (Fig. S2). Moreover, in both cases, the light scattering intensity decreased linearly on diluting the solutions (98% conversions) from 15.0 to 0.10 mg/mL (Fig. S3). These results indicate that PISA aggregates were stable with a critical aggregation concentration (CAC) below a 0.10 mg/mL. Thus, the solutions were diluted to 1.0 g/L for the DLS studies. As shown in Fig. 3b, PISA at DP_{target}=200 led to the formation of bimodal micelles with majority of D_h=97 nm and minority of 33 nm at dispersity of 0.17, and light scattering intensity of 200.2 kcps. The formation of bimodal aggregates was also observed during PISA at DP_{target}=100 to 98% conversion, with majority of D_h=55 nm and minority of 27 nm at dispersity of 0.082, and light scattering intensity (63.0 kcps) lower than the former.

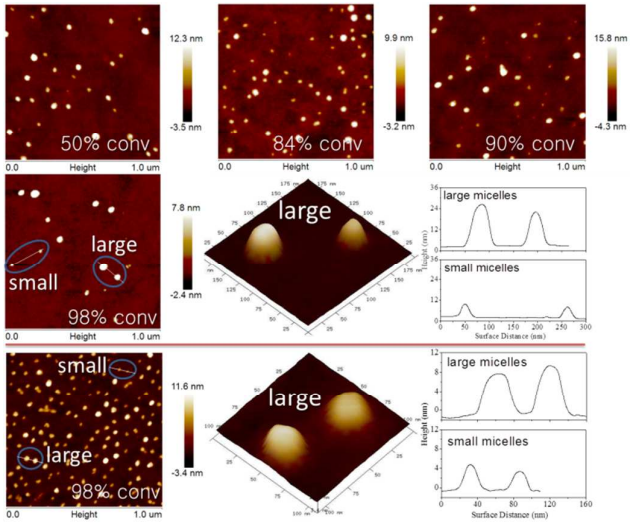

Fig. 4 AFM images of the micelles formed on polymerisation at $[DAAM]_0/[PHPMA166]_0/[SPTP]_0$ = 200/1/0.25 (*top*) and 100/1/0.25 (*bottom*) under the conditions of Fig. 2.

AFM (top of Fig. 4) and TEM (Fig. S4) confirmed formation of spherical micelles over the 50-98% conversions at DP_{target}= 200. These micelles exhibited bimodal size distribution over this range, consistent with above-discussed DLS observations. Typical AFM cross sections at a 98% conversion indicate rigid large micelles at height/diameter=0.33-0.36 and relatively soft small ones at a height/diameter=0.20-0.21. PISA at DP_{target}=100 to 98% conversion also led to typical bimodal size distribution (bottom in Fig. 4). Typical cross sections indicate large micelles at a height/diameter=0.17-0.21 and small ones at 0.13-0.14. These bimodal micelles are softer than the former ones. The bimodal size distribution is most presumably correlated to mild aqueous reaction circumstance. Currently, we cannot give a convincible evidence to explain this abnormal behaviour.

As shown in Fig. 5a, at a DP_{target}=200, their SEC traces are unimodal and symmetrical before 35% conversions. However, it was gradually broadened after onset of reaction acceleration, over which DAAM units were dehydrated and the rigid micelles were formed (Fig. 4). However, at a DP_{target}=100 (Fig. 5b), the SEC traces are unimodal and symmetrical to 98% conversions, where DAAM units were slightly hydrated (Fig. 2b) and swollen micelles were formed (Fig. 4). On one hand, a slight hydration in hydrophobic PISA-cores favoured mobility of growing-chain radicals and the permeation of residual monomer molecules to hydrophobic domains. Both led to closely equal opportunity of each growing radical to be attacked by monomer molecules, and thus low dispersity of growing chains.

As shown in Fig. 5c, the molecular weights increase linearly with conversions. Their plots are parallel to the corresponding theoretical ones although the molar masses are overestimated owing to the use of PMMA standards. Thus, all these aqueous dispersion RAFT processes were well controlled.

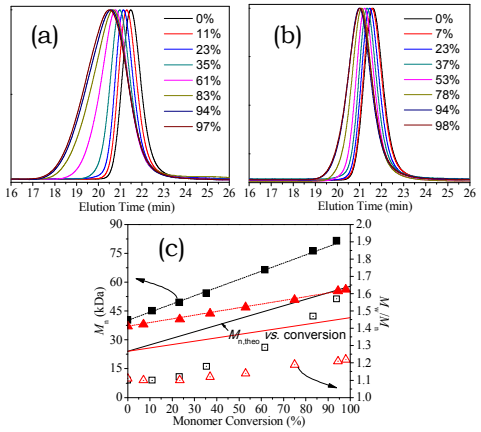

Fig. 5 SEC trace evolution during polymerisation at $[DAAM]_0/[PHPMA166]_0/[SPTP]_0$ = 200/1/0.25 (**a**) and 100/1/0.25 (**b**) under the conditions of Fig. 2; (**c**) the variation of molecular weights (M_n) and polydispersity indices (M_w/M_n) with monomer conversions at the feed molar ratios of 200/1/0.25 (*black*) and 100/1/0.25 (*red*).

In short, PISA was achieved by aqueous dispersion RAFT of DAAM using a water-soluble PHPMA macro-CTA under visible light irradiation at 25°C, which underwent dehydration, phase separation, micellization and reaction acceleration. Moreover, the slight hydration inside hydrophobic PISA-cores led to the low dispersity of the growing chains. Such behaviour inspired us to pursue a new class of NH_3^+-based reactive nanoparticles as to be discussed below.

Direct approach to interfacial NH_3^+-decorated nanoparticles

To elucidate the effectiveness in one-pot synthesis of reactive nanoparticles, minimal DAAM monomer in as-mentioned PISA at a DP_{target}=200 was replaced by NH_3^+-based AEAM monomer (Scheme 1), such that the core-forming block can be hydrated inside the hydrophobic PISA-cores.

Firstly, a reaction proceeded at $[AEAM]_0/[DAAM]_0$=20/180. As shown in Fig. 6a, the proton signals of PHPMA macro-CTA and both monomers are discernible by ^1H NMR in methanol-d_4. On irradiation, C**H**=C**H**$_2$ signals of both monomers decreased and signal *p* in PDAAM increased. These variations indicate the effectiveness of copolymerisation. Monomer conversions were determined according to Eqs. 3-4, where $I_{b,0}$, $I_{v,0}$, $I_{k,0}$ are initial integral signals *b*, *v*, *k*; $I_{b,t}$, $I_{k,t}$ are those at different time points.

$$Conversion_{DAAM} = \left(1 - \frac{I_{b,t}}{I_{k,t}} \times \frac{I_{k,0}}{I_{b,0}}\right) \times 100\% \quad (3)$$

$$Conversion_{AEAM} = \left(1 - \frac{I_{v,t}}{I_{k,t}} \times \frac{I_{k,0}}{I_{v,0}}\right) \times 100\% \quad (4)$$

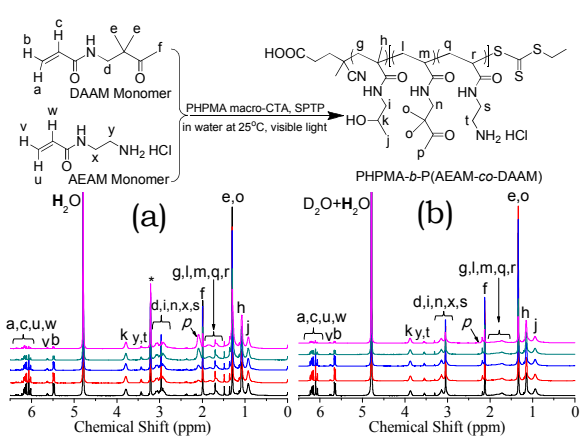

Fig. 6 ^{1}H NMR spectrum evolution upon aqueous copolymerisation at $[monomers]_0$= 0.5 M, $[AEAM]_0/[DAAM]_0$=20/180 and $[monomers]_0/[PHPMA_{166}]_0/[SPTP]_0$=200/1/0.25 under visible light irradiation at 25°C for 0, 8, 15, 28, 37 min (*from bottom to top*), in which spectra were recorded in methanol-d_4 (**a**) and D_2O (**b**).

Dehydration of DAAM units was probed by ^{1}H NMR in D_2O. As shown in Fig. 6b, signal *p* is weaker than that in methanol-d_4 (Fig. 6a) due to the dehydration of DAAM units. Nevertheless, signals *y* and *t* ($CH_2NH_3^+$ in AEAM monomer and unit) are discernible at high conversions. The results indicate hydration of AEAM units. Dehydration of DAAM units was determined according to Eq. 5, in which $I_{k,0}$, $I_{y,0}$, $I_{(d+i+x),0}$ are the initial integral signals; $I_{(d+i+n+x+s),t}$, $I_{k,t}$ and $I_{(y+t),t}$ are the integral signals at different time points; DAAM conversions determined in methanol-d_4 by Eq. 3 were used herein.

$$Dehydration = \left(1 - \frac{I_{(d+i+n+x+s),t} - 2 \times I_{k,t} - I_{(y+t),t}}{I_{(d+i+x),0} - 2 \times I_{k,0} - I_{y,0}} \times \frac{I_{k,0}}{I_{k,t}}\right) \times \frac{1}{Conversion_{DAAM}} \times 100\% \quad (5)$$

As shown in Fig. 7a, at a $[AEAM]_0/[DAAM]_0$=10/190, 14 min of irradiation led to a 23% DAAM conversion, in which reaction of AEAM was negligible. Hence, the reaction started from the formation of PDAAM core-forming block. 36% DAAM and 10% AEAM were consumed after irradiation for 17 min. Reaction of DAAM accelerated after 46% conversions, which is comparable to that (45%) in the homopolymerisation at DP_{target}=200 (Fig. 2). Thereafter, both the monomers polymerized, indicated by the simultaneous conversions. DAAM consumed faster than AEAM, despite active nature of AEAM under such conditions (Fig. S5).

In the reactions at $[AEAM]_0/[DAAM]_0$=20/180 (Fig. 7b) and 30/170 (Fig. 7c), DAAM reaction acceleration started from 56% and 67% conversions, respectively. Entirely different from that at 10/190, irradiation initiated simultaneous copolymerisation and AEAM reaction acceleration also occurred after 49%, 55% conversions. Reaction acceleration was observed by Armes,[54] in copolymerisation of a water-soluble monomer and a water-insoluble monomer using a water-soluble macro-CTA. These results indicate effective enrichment of both monomers due to the slight hydration inside their PISA-cores.

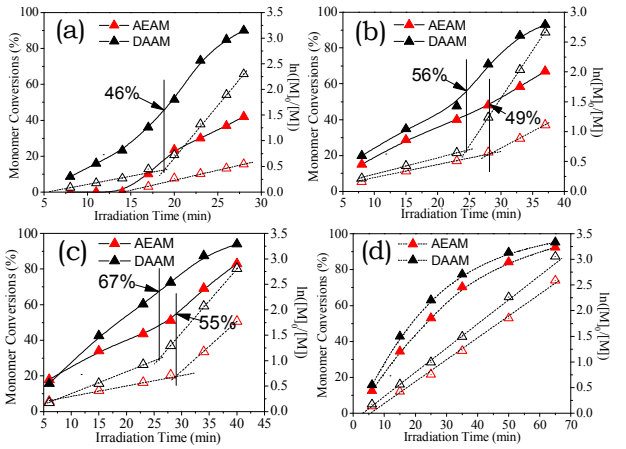

Fig. 7 Kinetic curves of RAFT copolymerisation at feed ratios $[AEAM]_0/[DAAM]_0$=10/190 (**a**), 20/180 (**b**), 30/170 (**c**), and 40/160 (**d**) under the conditions of Fig. 6.

However, in reaction at $[AEAM]_0/[DAAM]_0$=40/160 (Fig. 7d), semilogarithmic plots increased linearly to 94% AEAM and 96% DAAM conversions. The copolymer was soluble in the reaction solution, as judged by transparent solution at constant integral signals in D_2O and methanol-d_4 (Fig. S6). These results indicate the reaction in a homogeneous solution. Reaction acceleration did not occur under such aqueous conditions.

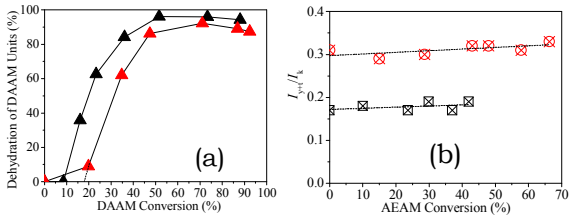

Fig. 8 (**a**) Dehydration of DAAM units with DAAM conversions; (**b**) hydration of AEAM units (based on $CH_2NH_3^+$ integral signals *y*+*t* using $CH(OH)CH_3$ signal *k* standard, I_{y+t}/I_k) during the reactions at $[AEAM]_0/[DAAM]_0$=10/190 (*black*) and 20/180 (*red*).

As shown in Fig. 8a, at a $[AEAM]_0/[DAAM]_0$=10/190, the dehydration of DAAM units occurred after 10% conversions, comparable to that in homopolymerisation at DP_{target}=200 (Fig. 2b), but DAAM units were slightly hydrated at high conversions. In contrast, at $[AEAM]_0/[DAAM]_0$=20/180, dehydration started from 18% DAAM conversions, and more than 10% DAAM units were hydrated at final conversions. These results demonstrate that incorporation of AEAM units into the core-forming block enhanced hydration of their hydrophobic PISA-cores.

Moreover, the integral signals *y* and *t* ($CH_2NH_3^+$ in AEAM monomer and unit) maintained essentially constant up to the ultimate conversions in both reactions (Fig. 8b). These results indicate that the AEAM units are accessible to water, negligible encapsulation into hydrophobic PISA-domains. These results indicate that the simultaneous self-assembly and chain growth favoured the mobility of growing chains, leading to sufficient

adjustment of newly-added ionic AEAM units outward to core-shell interfaces while the hydrophobic DAAM units tended to collapse into PISA-cores. Such behaviour led to the selective self-assembling into nanostructures with the ideal accessibility of reactive NH_3^+-motifs to be accessible to substance in water.

The effect of water-soluble AEAM units on phase transition was elucidated by DLS. At $[AEAM]_0/[DAAM]_0$=10/190 (Fig. 9a), phase separation started at 40% DAAM-conversion, behind the onset of dehydration (10%) but ahead of the onset of reaction acceleration (46%). Whereas, at a $[AEAM]_0/[DAAM]_0$=20/180, phase transition started at 50% DAAM-conversion, behind the former because of enhanced hydration of core-forming block.

To illustrate colloidal stability in water, the solutions were dialyzed against water to remove the residual monomers and then lyophilized. The solids were dispersed in water to a 1.0 mg/mL and re-adjusted to pH 3.8. DLS confirmed essentially the same micelles as the originals. These results illustrate the colloidal stability of these PISA-micelles.

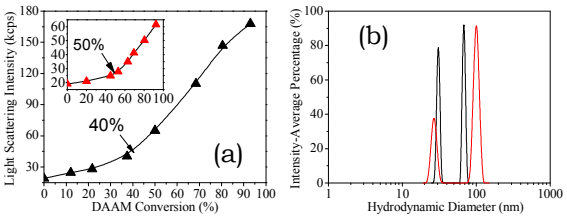

Fig. 9 (**a**) The variation of light scattering intensity upon copolymerisation at $[AEAM]_0/[DAAM]_0$=10/190 (*black*) and 20/180 (*red*) under the conditions of Fig 6, in which laser was decreased down to 20%; (**b**) the size distribution profiles of the PISA-micelles.

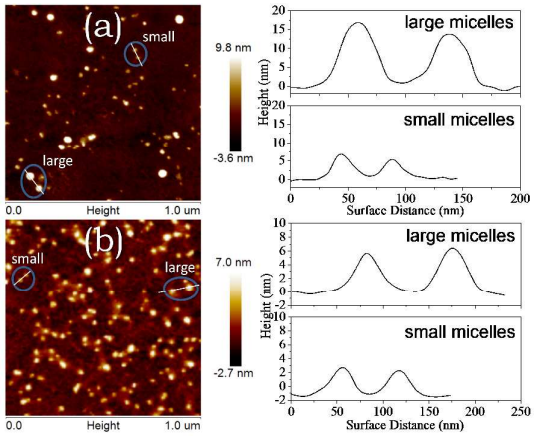

Fig. 10 AFM images of the PISA-micelles formed at $[AEAM]_0/[DAAM]_0$=10/190 (**a**) and 20/180 (**b**) under the conditions of Fig. 6.

As shown in Fig. 9b, PISA at $[AEAM]_0/[DAAM]_0$=10/190 to 93% DAAM and 46% AEAM conversion led to bimodal micelles at D_h=68 and 31 nm with a dispersity of 0.16, with an intensity of 71.7 kcps. The micelles are smaller and swollen than those formed in homopolymerisation at DP_{terget}=200 (Fig. 3). These micelles were stable after diluted to 0.10 g/L (Fig. S7). In contrast, at $[AEAM]_0/[DAAM]_0$ =20/180 to 95% DAAM and 67% AEAM conversions, bimodal swollen micelles with the majority at D_h=101 nm and minority at D_h=27 nm and dispersity of 0.26, were observed. A low light scattering intensity (30.1 kcps) was detected due to the hydration of hydrophobic PISA-cores.

AFM (Fig. 10) confirmed the formation of spherical micelles. At $[AEAM]_0/[DAAM]_0$=10/190, these bimodal profiles indicate micelles at a height/diameter=0.20-0.21 for the large ones and a 0.13-0.15 for the small ones. In contrast, the PISA-micelles formed at $[AEAM]_0/[DAAM]_0$=20/180 was clearly softer than the formers. Their typical bimodal cross sections indicated the height/diameter of 0.06-0.08.

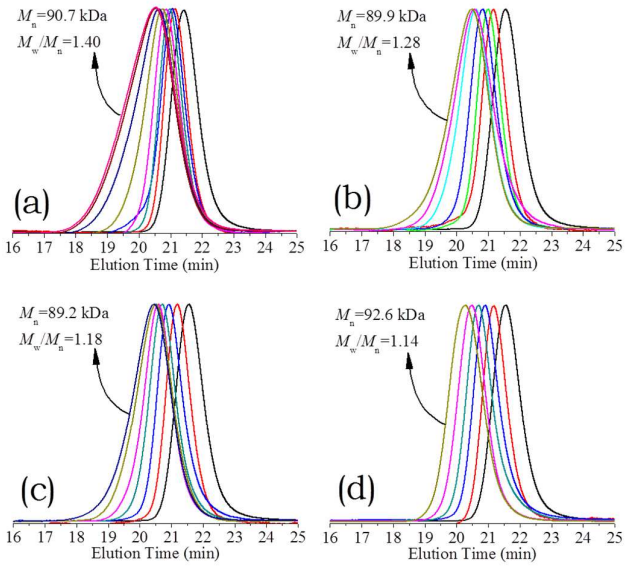

Fig. 11 SEC trace evolution upon copolymerisation in water at $[monomers]_0$=0.5 M and DP_{target}=200 under visible light irradiation at 25°C, with the feed ratio $[AEAM]_0/[DAAM]_0$ of 10/190 up to 93% DAAM and 46% AEAM conversions (**a**), 20/180 up to 95% DAAM and 67% AEAM conversions (**b**), 30/170 up to 94% DAAM and 81% AEAM conversions (**c**) and 40/160 up to 96% DAAM and 94% AEAM conversions (**d**).

As shown in Fig. 11, all the SEC traces are unimodal and symmetrical before phase separation but gradually broadened after the onset of reaction acceleration. Polydispersity (M_w/M_n) of final samples decreased from 1.40 to 1.28, 1.18 and 1.14 on the increase of $[AEAM]_0/[DAAM]_0$ from 10/190 to 40/160. The variations confirm that the slight hydration inside hydrophobic PISA-cores indeed exerts crucial control over the dispersity.

Accessibility and reactivity of NH_3^+-decorated nanoparticles

Zeta potential (ζ) represents the surface charge of particles in relation to surrounding conditions in a given medium.[55] Thus, inspection of zeta potential variation with conversions allows convenient discrimination of the accessibility of NH_3^+-motifs. Accordingly, a range of reaction solutions at $[AEAM]_0/[DAAM]_0$ =10/190 and 20/180 at different conversions were selected. These solutions were dialyzed against water to remove the residual monomers and then lyophilized. Solids were dispersed in water to 1.0 mg/mL and re-adjusted to pH 3.8 at 20°C for aqueous electrophoresis studies.

As shown in Fig. 12, all these micelles show positive zeta potentials, confirming the ionization of AEAM units. Moreover, ζ values increased with the monomer conversions, in which ζ values increased from +9.8 to +21.0 mV on increase of DAAM

conversions from 68% to 93% at a $[AEAM]_0/[DAAM]_0$ =10/190, and from +15.0 to +32.1 mV on increase from 69% to 95% at a $[AEAM]_0/[DAAM]_0$=20/180. The results confirm that the NH_3^+-motifs decorate surrounding the core-shell interfaces. These results are consistent with the complete AEAM-hydration but significant DAAM-dehydration at high conversions as judged by ^{1}H NMR (Fig. 8). The interface distribution of these NH_3^+-motifs endows the ideal accessibility to substrates in water.

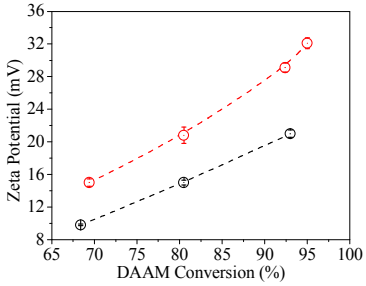

Fig. 12 Aqueous electrophoresis data obtained for the PISA-micelles at varied DAAM conversions at $[AEAM]_0/[DAAM]_0$=10/190 (*black*) and 20/180 (*red*) in water at pH 3.8.

On one hand, simultaneous process of in situ assembly and chain growth favoured adjustment of growing chains. On the other hand, hydrophilic/hydrophobic natures of AEAM/DAAM units determine either hydration or dehydration. Both effects induced timely and selective self-assembly of the core-forming block, in which hydrophobic DAAM units tended to collapse to PISA-cores while AEAM units tended to enrich outward to the core-shell interfaces, leading to interfacial decoration of NH_3^+-motifs. Electrostatic repulsion force of interfacial NH_3^+-motifs enhanced colloidal stability against coacervation in water.[28, 55]

To illustrate the reactivity, these NH_3^+-motifs were further conjugated with PDCA to form typical terdendate ligand motifs after adjusted to pH 9.8 (Scheme 1). These hydrophobic ligand motifs have high coordination constants with ferrous, cobalt, nickel, copper ions and zinc ions.[39, 40] Moreover, their chemical environment can be tuned by the self-assembly surrounding hydrophobic cores,[6-8] and thus are promising as precursors of enzyme-inspired aqueous catalysts.[6-9] Zn(II)-coordination was selected to illustrate the reactivity of the interfacial-decorated reactive nanoparticles (see Scheme 1).

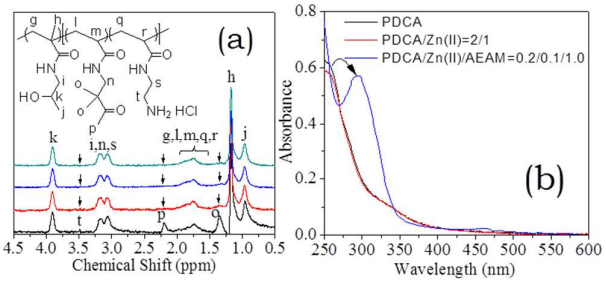

Fig. 13 (**a**) ^{1}H NMR spectra of the resulting micelles at $[AEAM]_0/[DAAM]_0$=20/180 (1.0 mg/mL in D_2O at pH 3.8) (*black*) after adding NaOD solution to pH 9.8 (*red*), conjugation with PDCA ($[AEAM]_0/[PDCA]_0$=1/0.2, *blue*) and coordination ($[AEAM]_0/[PDCA]_0/[Zn(II)]_0$ =1/0.2/0.1, *green*); (**b**) the UV-vis spectra of PDCA, PDCA/Zn(II) and the micelles after the simultaneous PDCA-conjugation and Zn(II)-coordination.

As shown in Fig. 13a, AEAM co-units have been dehydrated after conversion into NH_2-motifs, indicated by the attenuation of CH_2NH_2 signals *t*. Alkalization induced the dehydration of initially-hydrated DAAM units, leading to the attenuation of signals *p* and *o*. These results implied that neighbouring NH_3^+-motifs enhanced the hydration of DAAM units. AEAM/DAAM signals disappeared after simultaneous PDCA-conjugation and Zn(II)-coordination. Hydrophobic dative bonds were confirmed by the red-shift to characteristic UV band of Zn(II)-coordinated ligand motifs (Fig. 13b). Zn(II)-coordination of the AEAM-PDCA motifs was confirmed by ^{1}H NMR and UV-vis spectroscopy of their corresponding small compounds (Fig. S9).

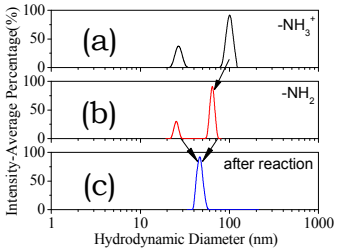

Fig. 14 Size distribution profiles of PISA micelles formed at a $[AEAM]_0/[DAAM]_0$=20/180 (1.0 mg/mL in water) at pH 3.8 (**a**) and pH 9.8 (**b**), and those after PDCA-conjugation and Zn(II)-coordination at a $[AEAM]_0/[PDCA]_0/[Zn(II)]_0$=1/0.2/0.1 (**c**).

Furthermore, as shown in Fig. 14, the swollen PISA-micelles were shrunken after deionization, in which the minors shrank from D_h=23-32 to 21-28 nm, the majors from D_h=83-126 to 55-74 nm, and the light scattering intensity increased from 30.1 to 51.5 kcps. Moreover, hydrophobic dative ligand motifs led to the shrinkage of large micelles and the coacervation of small micelles into rigid micelles at D_h=40-57 nm with the unimodal dispersity of 0.066, and an increase of intensity to 102.4 kcps. The aggregation of the highly-swollen small micelles was most presumably induced by the dative-bonded inter-particle cross-linking. Currently, we cannot give a convincing evidence for this behaviour. However, at least, the results demonstrate the reconstruction of these PISA-micelles.

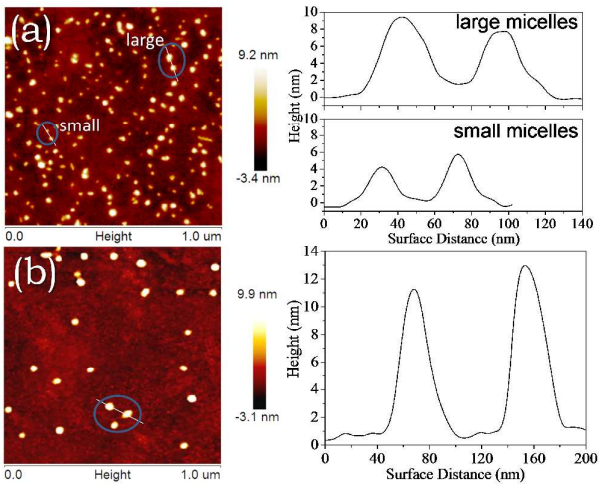

Fig. 15 AFM height (*left*) and the cross sections (*right*) of (**a**) the PISA-micelles formed at $[AEAM]_0/[DAAM]_0$=20/180 after alkalization to pH 9.8, and (**b**) Zn(II)-hybridized micelles.

AFM (Fig. 15) visualized the formation of spherical micelles after the deionization to NH_2-motifs. The typical cross sections show height/diameter=0.17 of large micelles and 0.13 of small ones. These micelles are more rigid than those in acidic water at pH 3.8 (height/diameter=0.06-0.08, Fig. 10). These results are consistent with those observed by DLS. Moreover, small micelles aggregated and the large micelles were shrunken into compact nanoparticles with a height/diameter=0.21-0.22 after these simultaneous PDCA-conjugation and Zn(II)-coordination. Consequently, functional dative metal centres have decorated surrounding the core-shell interfaces. Such unique architecture endows function dative metal centres with both huge specific surface area and excellent accessibility to substrates in water. Self-assembly of amphiphilic block copolymers in water suffers from the encapsulation of hydrophobic reactive motifs in core-forming block. According to above-discussed results, the new strategy effectively circumvented this accessibility problem.

These hybridized PISA-particles are stable in water owing to steric stabilization of water-soluble shells. DLS unveiled the same sizes and dispersity as initials after keeping the solutions at room temperature for 2 months. Both the huge assessable specific surface area of functional dative metal centres and excellent colloidal stability provided fascinating potentials of these new reactive nanoparticles as the precursors of enzyme-inspired aqueous catalysts.[6-9]

Conclusions

This article described a fast PISA via aqueous dispersion RAFT polymerisation of a commercially available specialty monomer DAAM using a water-soluble PHPMA macro-CTA under visible light irradiation at 25°C. Polymerisation induced sequentially dehydration, phase separation and reaction acceleration inside spherical micelles. More importantly, a slight hydration inside hydrophobic PISA-cores led to narrowing-down of molar mass distribution of the block copolymer. Similarly, incorporation of minimal AEAM units into core-forming block induced the slight hydration of hydrophobic core-forming block, thus leading to a low dispersity of PHPMA-*b*-P(AEAM-*co*-DAAM) statistic-block copolymers.

More importantly, simultaneous in situ assembly and chain growth favoured adjustment of growing-chain conformations, in which the newly-added water-soluble AEAM co-units tended to shift outward to the core-shell interfaces while DAAM units tended to collapse into hydrophobic PISA-cores. This led to the timely and selective self-assembly of core-forming block into new reactive nanoparticles whose interfacial NH_3^+-motifs are accessible to substrates in water. Hence, simultaneous PDCA-conjugation and Zn(II)-coordination led to the decoration of functionalized dative metal centres surrounding the core-shell interfaces. The PISA-nanostructures are sterically stabilized by water-soluble PHPMA-shells. The structures endow functional dative metal centres with huge accessible specific surface area. Thus, these reactive nanoparticles are promising as precursors of metalloenzyme-inspired aqueous catalysts.[6-9]

Acknowledgements

This research work was supported by National Natural Science Foundation of China (21274097, 21474069, 21334004) and the Priority Academic Program Development of Jiangsu Higher Education Institutions.

Notes and references

1. M. J. Monteiro and M. F. Cunningham, *Macromolecules*, 2012, **45**, 4939-4957.
2. Z. L. Tyrrell, Y. Shen and M. Radosz, *Prog. Polym. Sci.*, 2010, **35**, 1128-1143.
3. B. Charleux, G. Delaittre, J. Rieger and F. D'Agosto, *Macromolecules*, 2012, **45**, 6753-6765.
4. J. T. Sun, C. Y. Hong and C. Y. Pan, *Soft Matter*, 2012, **8**, 7753-7767.
5. N. J. Warren and S. P. Armes, *J. Am. Chem. Soc.*, 2014, **136**, 10174-10185.
6. D. E. Bergbreiter, *ACS Macro Lett.*, 2014, **3**, 260-265.
7. E. Huerta, P. J. M. Stals, E. W. Meijer and A. R. A. Palmans, *Angew. Chem. Int. Ed.*, 2013, **52**, 2906-2910.
8. T. Terashima, T. Mes, T. F. A. De Greef, M. A. J. Gillissen, P. Besenius, A. R. A. Palmans and E. W. Meijer, *J. Am. Chem. Soc.*, 2011, **133**, 4742-4745.
9. N. Madhavan, C. W. Jones and M. Weck, *Acc. Chem. Res.*, 2008, **41**, 1153-1165.
10. J. Chiefari, Y. K. Chong, F. Ercole, J. Krstina, J. Jeffery, T. P. T. Le, R. T. A. Mayadunne, G. F. Meijs, C. L. Moad, G. Moad, E. Rizzardo and S. H. Thang, *Macromolecules*, 1998, **31**, 5559-5562.
11. G. Moad, E. Rizzardo and S. H. Thang, *Acc. Chem. Res.*, 2008, **41**, 1133-1142.
12. C. J. Ferguson, R. J. Hughes, D. Nguyen, B. T. T. Pham, R. G. Gilbert, A. K. Serelis, C. H. Such and B. S. Hawkett, *Macromolecules*, 2005, **38**, 2191-2204.
13. C. J. Ferguson, R. J. Hughes, B. T. T. Pham, B. S. Hawkett, R. G. Gilbert, A. K. Serelis and C. H. Such, *Macromolecules*, 2002, **35**, 9243-9245.
14. J. Rieger, F. Stoffelbach, C. Bui, D. Alaimo, C. Jerome and B. Charleux, *Macromolecules*, 2008, **41**, 4065-4068.
15. J. Rieger, G. Osterwinter, C. Bui, F. Stoffelbach and B. Charleux, *Macromolecules*, 2009, **42**, 5518-5525.
16. E. Groison, S. Brusseau, F. D'Agosto, S. Magnet, R. Inoubli, L. Couvreur and B. Charleux, *Acs Macro Lett.*, 2012, **1**, 47-51.
17. T. Boursier, I. Chaduc, J. Rieger, F. D'Agosto, M. Lansalot and B. Charleux, *Polym. Chem.*, 2011, **2**, 355-362.
18. Z. An, Q. Shi, W. Tang, C.-K. Tsung, C. J. Hawker and G. D. Stucky, *J. Am. Chem. Soc.*, 2007, **129**, 14493-14499.
19. A. Blanazs, J. Madsen, G. Battaglia, A. J. Ryan and S. P. Armes, *J. Am. Chem. Soc.*, 2011, **133**, 16581-16587.
20. S. Sugihara, A. Blanazs, S. P. Armes, A. J. Ryan and A. L. Lewis, *J. Am. Chem. Soc.*, 2011, **133**, 15707-15713.
21. A. Blanazs, A. J. Ryan and S. P. Armes, *Macromolecules*, 2012, **45**, 5099-5107.
22. A. Blanazs, R. Verber, O. O. Mykhaylyk, A. J. Ryan, J. Z. Heath, C. W. I. Douglas and S. P. Armes, *J. Am. Chem. Soc.*, 2012, **134**, 9741-9748.
23. P. Chambon, A. Blanazs, G. Battaglia and S. P. Armes, *Macromolecules*, 2012, **45**, 5081-5090.

24. V. Ladmiral, M. Semsarilar, I. Canton and S. P. Armes, *J. Am. Chem. Soc.*, 2013, **135**, 13574-13581.
25. L. P. D. Ratcliffe, A. J. Ryan and S. P. Armes, *Macromolecules*, 2013, **46**, 769-777.
26. M. Semsarilar, V. Ladmiral, A. Blanazs and S. P. Armes, *Langmuir*, 2013, **29**, 7416-7424.
27. N. J. Warren, O. O. Mykhaylyk, D. Mahmood, A. J. Ryan and S. P. Armes, *J. Am. Chem. Soc.*, 2014, **136**, 1023-1033.
28. J. R. Lovett, N. J. Warren, L. P. Ratcliffe, M. K. Kocik and S. P. Armes, *Angew. Chem. Int. Ed.* 2015, **54**, 1279-1283.
29. G. Liu, Q. Qiu, W. Shen and Z. An, *Macromolecules*, 2011, **44**, 5237-5245.
30. W. Zhou, Q. Qu, W. Yu and Z. An, *ACS Macro Lett.*, 2014, **3**, 1220-1224.
31. W. Zhou, Q. Qu, Y. Xu and Z. An, *ACS Macro Lett.*, 2015, 495-499.
32. C. A. Figg, A. Simula, K. A. Gebre, B. S. Tucker, D. M. Haddleton and B. S. Sumerlin, *Chem. Sci.*, 2015, **6**, 1230-1236.
33. G. Delaittre, M. Save and B. Charleux, *Macromol. Rapid Commun.*, 2007, **28**, 1528-1533.
34. L. Hou, K. Ma, Z. An and P. Wu, *Macromolecules*, 2014, **47**, 1144-1154.
35. G. Liu, Q. Qiu and Z. An, *Polym. Chem.*, 2012, **3**, 504-513.
36. W. Shen, Y. Chang, G. Liu, H. Wang, A. Cao and Z. An, *Macromolecules*, 2011, **44**, 2524-2530.
37. X. Tang, J. Han, Z. Zhu, X. Lu, H. Chen and Y. Cai, *Polym. Chem.*, 2014, **5**, 4115-4123.
38. C. W. Scales, Y. A. Vasilieva, A. J. Convertine, A. B. Lowe and C. L. McCormick, *Biomacromolecules*, 2005, **6**, 1846-1850.
39. B. de Bruin, E. Bill, E. Bothe, T. Weyhermuller and K. Wieghardt, *Inorg. Chem.*, 2000, **39**, 2936-2947.
40. G. Koz, N. Ozdemir, D. Astley, M. Dincer and S. T. Astley, *J. Mol. Struct.*, 2010, **966**, 39-47.
41. J. Y. Tong, Y. Shi, G. H. Liu, T. Huang, N. Xu, Z. G. Zhu and Y. L. Cai, *Macromol. Rapid Commun.*, 2013, **34**, 1827-1832.
42. A. Henne, A. Hesse, M. Jacobi, G. Wallbillich, B. Bronstert, Patent US 4719297, 1988.
43. X. W. Xu, A. E. Smith, S. E. Kirkland and C. L. McCormick, *Macromolecules*, 2008, **41**, 8429-8435.
44. J. Z. Du and S. P. Armes, *Langmuir*, 2008, **24**, 13710-13716.
45. E. S. Read, K. L. Thompson and S. P. Armes, *Polym. Chem.*, 2010, **1**, 221-230.
46. Y. Shi, H. Gao, L. Lu and Y. Cai, *Chem. Commun.*, 2009, 1368-1370.
47. Y. Shi, G. Liu, H. Gao, L. Lu and Y. Cai, *Macromolecules*, 2009, **42**, 3917-3926.
48. G. Liu, H. Shi, Y. Cui, J. Tong, Y. Zhao, D. Wang and Y. Cai, *Polym. Chem.*, 2013, **4**, 1176-1182.
49. H. Lin, D. Zhang, P. G. Alexander, G. Yang, J. Tan, A. W.-M. Cheng and R. S. Tuan, *Biomaterials*, 2013, **34**, 331-339.
50. B. D. Fairbanks, M. P. Schwartz, A. E. Halevi, C. R. Nuttelman, C. N. Bowman and K. S. Anseth, *Adv. Mater.*, 2009, **21**, 5005-5010.
51. B. D. Fairbanks, M. P. Schwartz, C. N. Bowman and K. S. Anseth, *Biomaterials*, 2009, **30**, 6702-6707.
52. Q. L. Li, C. Q. Gao, S. T. Li, F. Huo and W. Q. Zhang, *Polym. Chem.*, 2014, **5**, 2961-2972.
53. Y. Su, X. Xiao, S. Li, M. Dan, X. Wang and W. Zhang, *Polym. Chem.*, 2014, **5**, 578-587.
54. L. P. D. Ratcliffe, A. Blanazs, C. N. Williams, S. L. Brown and S. P. Armes, *Polym. Chem.*, 2014, **5**, 3643-3655.
55. A. Mikolajczyk, A. Gajewicz, B. Rasulev, N. Schaeublin, E. Maurer-Gardner, S. Hussain, J. Leszczynski and T. Puzyn, *Chem. Mater.*, 2015, **27**, 2400-2407.

TOC Graphic

Enzyme inspired interface-decorated media-accessible reactive nanoparticles are now available *via* PISA by aqueous dispersion RAFT of commodity-DAAM with minimal NH_3^+-monomer.